INTERNATIONAL JOURNAL OF
COASTAL, OFFSHORE & MEDIUMAL ENGINEERING IJCOE Vol.11/No. 1/Winter 2026 (91-102)

Available online at: www. ijcoe.org

Development of Oceanic Numerical Model for Persian Gulf (part 2)

Mehri Fallahi[1], Masoud Sadrinasab[2*]

[1] *Instructor of Physics Lab, , Department of Agriculture Machinery Engineering, Faculty of Agricultural Engineering and Technologies, Collage of Agriculture & Natural Resources, Tehran University, Tehran, Iran, mehri_fallahi@ut.ac.ir*

[2*] *Associate Professor, Department of Environment Engineering, school of Graduate Environment, university of Tehran , Tehran, Iran masoud.sadri@ut.ac.ir*

ARTICLE INFO

Article History:
Received:17 Sep 2025
Accepted :11 Jan 2026

Keywords:
Persian Gulf
numerical model
primitive equations
sigma vertical coordinate
forced tide.

ABSTRACT

This study presents the development of a three-dimensional numerical model, the Persian Gulf Oceanic Model (ZSF974), designed to predict oceanographic parameters in the Persian Gulf, along with the results of its validation. The model is based on the primitive equations formulated in a spherical coordinate system with a sigma vertical coordinate. The model equations are solved numerically using the finite difference method: the Lax–Wendroff scheme for advective terms, the DuFort–Frankel scheme for diffusive terms, and the Matsuno scheme to control computational instabilities. The mesh employed is a modified Arakawa C grid. The model accommodates irregular bathymetry and supports variable resolution in both horizontal and vertical directions. Model accuracy was enhanced by optimizing the execution process and by properly applying Nihoul's (1977) theory on the wind-induced surface stress's effect on subsurface layers. After validating the model in idealized laboratory basins against established principles of physical oceanography and previous research, it was applied to the real-world environment of the Persian Gulf. Key results from the model's implementation include a counterclockwise water circulation, the presence of an amphidromic point, the dominance of tidal forces, and the influence of the Arvandrud and Mond rivers. Notably, this riverine impact is significant along the coasts of the United Arab Emirates. The model successfully simulates the general behavior of the oceanic environment in response to various forcing mechanisms. However, long-term simulations indicate that the open boundary conditions require modification and that real tidal forcing should be incorporated. Overall, the model shows significant potential for further development to yield more accurate simulations and robust conclusions.

1. Introduction

While oceans and seas contain over 97% of the Earth's water, it is primarily saltwater. They are, however, the fundamental source of the planet's freshwater through the hydrological cycle, which sustains all life. They play a vital role in regulating the global climate. Therefore, studying oceanic phenomena is essential for the sustainable management of this vast resource.

The Persian Gulf is a water basin situated the south of Iran (Figure 1), extends from 24° to 30°30' N latitude and from 48° to 56°25' E longitude.

Its coasts and continental shelf are rich in oil and gas reserves. This region also serves as a major global transit for oil, with the Persian Gulf exporting over 60% of the world's seaborne oil. Consequently, the Gulf holds immense economic and political significance increasing the value of research across various fields. In this context, research into the Gulf' physical

parameters, it's climate and coastal impacts, and broader oceanic phenomena, is of paramount importance.

This semi-enclosed basin, characterized by high temperature and salinity, is connected to the open ocean via the Strait of Hormuz. Investigating the impact of these conditions on marine life and pollution within the basin is a key research topic.

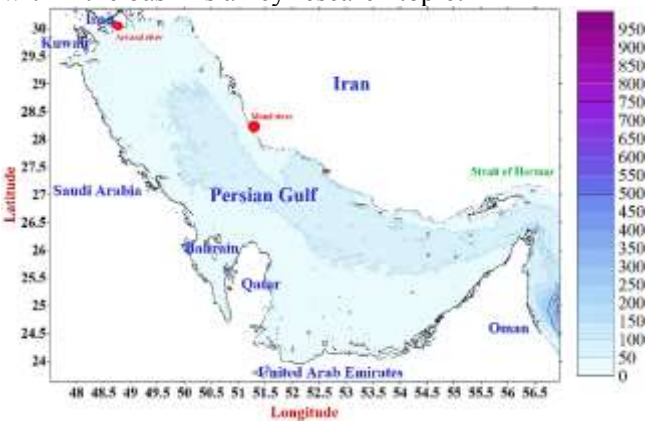

Figure 1- Location of the Persian Gulf

While satellite data analysis is a primary methods for study oceanic phenomena, satellites provide information only about surface waters. On the other hand, in-situ instruments, such as floating buoys, provide scattered data on physical parameters. Although, the governing equations can establish relationships between these disparate data points, they lack analytical solutions. Therefore, numerical methods provide the best means of solving them.

Numerical modeling describes atmospheric or oceanic systems by solving their governing equations numerically. A numerical model can explain a system's overall behavior in response to various forcings, predict or calculate parameters, and ultimately make the dynamics of a water basin comprehensible and analyzable. Model outputs are inherently subject to error. Nevertheless, by employing appropriate numerical methods, their accuracy can be improved to yield acceptable solutions.

The following section summarizes previous research conducted in the Persian Gulf using numerical models. In 1992, **Khaleghi Zavare** developed a non-linear barotropic model for the Persian Gulf. This model is based on the integration of shallow water equations in the vertical direction and is sensitive to the earth's rotation and the effects of bathymetric variations. The model was designed to determine the response of the Persian Gulf to wind and tidal forces through numerical simulation [1]. In 1994, **Zamanian** used a two-layer model to study the currents of the Persian Gulf. This model was based on the primitive equations in a Cartesian coordinate system with a sigma vertical coordinate. In addition to determining the current fields caused by wind and tides, this model predicts temperature and salinity in two layers, vertical velocity at a specified level, and sea surface height at the grid points [2]. **Sadrinasab and Kenarkoohi** (2009) examined the sound speed profile in different layers of the Persian Gulf. In this study, a three-dimensional hydrodynamic model (COHERENS) is employed in a fully prognostic mode to derive sound speed profiles in the Persian Gulf. Results of the model show that sound speed in the Persian Gulf depends mainly on temperature in the surface layer, whereas the bottom layer as well as the southern part of the Gulf depend on both temperature and salinity [3]. Sadrinasab, (2009) employed the COHERENS model as a three-dimensional hydrodynamic model to investigate coastal upwelling in the northern Persian Gulf with a horizontal resolution of 4 minutes of latitude and longitude. The findings showed that more kinetic energy accumulated along the Iranian coasts and also, a seasonal thermocline is evident with a surface to bottom temperature difference of around 12°C in summer. [4]. **Pous et al.** (2012) used a homogeneous shallow-water model with a free surface to study the tidal circulation in the Persian Gulf. The numerical finite-difference model includes harmonic diffusion of horizontal momentum and quadratic bottom friction. High-precision bathymetric data were used to represent the bottom topography. They found that tidal currents can be strong in the Strait of Hormuz and in shallow areas, thus having a significant effect on the region's hydrology. The residual currents are weak and therefore negligible for large-scale circulation over long periods [5]. **Azizpour et al**. (2014), conducted a study on the physical oceanographic properties of the Persian Gulf, the Strait of Hormuz, and the Sea of Oman based on CTD data. In this study, the spatial and temporal distributions of temperature, salinity, and density were investigated. They concluded that in summer, the water column was strongly stratified at deep stations and relatively well mixed at shallow stations. They also found that strong and weak thermocline layers were formed in summer ($\Delta T \approx 12$ °C) and winter ($\Delta T \approx 6$ °C) at deep stations, respectively [6]. **Delbari and Sheikhbahaei** (2020) numerically studied the propagation of underwater sound waves using the differential square method. In this study, the Differential Quadrature (DQ) method was applied for the numerical solution of underwater acoustic waves for the first time. Two experimental test cases were used to validate the two-dimensional wave model: first, the numerical results were verified against the analytical solution, and second, the applicability of the method in a complex domain was demonstrated. Comparisons confirmed the efficiency, accuracy, and robustness of the Differential Quadrature method for acoustic wave simulation [7]. **Mahpeykar and Khalilabadi** (2021) investigated the effect of wind speed and direction on evaporation rate in the Persian Gulf—assuming no water inflow to the basin—using numerical modeling. The results showed that wind direction has only a minor effect on evaporation,

whereas wind speed causes significant changes in both evaporation rate and water level. These changes are nonlinearly related to water temperature, such that in summer, as temperature increases, the evaporation rate increases more rapidly [8]. **Hosseini and Soltanpour** (2021) used the Flow Model (FM) module of MIKE 21 software (DHI, 2012) to investigate the characteristics of tidal wave propagation in the Persian Gulf. Their study indicated that tidal waves propagate from the Arabian Sea and the Gulf of Oman into the Persian Gulf through the Strait of Hormuz. Although the continental shelf resonance frequency of the basin is close to the period of diurnal constituents, the results showed that the tide is mainly mixed semidiurnal. The numerical experiments revealed that the Coriolis force, in combination with the geometry of the Persian Gulf, results in the generation of different amphidromic systems of diurnal and semidiurnal constituents. Moreover, the configuration of the bathymetry of the Persian Gulf—with a shallow zone at the closed end of the basin, extending longitudinally along the southern half (asymmetric cross-section)—leads to deformation of incoming and reflected tidal Kelvin waves and, consequently, to the shifting of amphidromic points [9]. **Pirooznia et al.** (2022) calibrated the MIKE21 oceanic numerical model for the Persian Gulf and the Gulf of Oman in order to improve the simulated surface currents obtained from the model. The calibration was performed through data assimilation of the model with altimetry and hydrographic observations using variational data assimilation, where the weights of the objective functions were defined based on the type of observations and optimized using metaheuristic optimization methods. According to the results, the calibration of the model generally led the model results closer to the observations. They showed that the kinetic energy produced by sea surface currents could be used for generating electricity in the Oman Sea and near Jask harbor [10].

Fallahi et al. (2019) designed a "Five-Layer Numerical Ocean Model of the Persian Gulf" with the aim of predicting physical parameters in the basin [11]. During the process of refining and enhancing the model, a laboratory-scale ocean basin was configured to resemble the Persian Gulf. A two-year simulation showed that the basin is dominated by semidiurnal tidal forcing, which prevails over wind stress and density-driven forces [12]. The consistency of the results with fundamental ocean physics and previous research provided a solid foundation for further model development.

The Persian Gulf, due to the extensive maritime boundary it provides for Iran, is of particular importance with respect to economic, tourism, and strategic activities. In addition, due to its unique geographical position, it has special strategic and economic value in the western part of Asia. Therefore, any research on this basin is considered highly important and strategic for planning purposes.

Since numerical modeling can be a powerful scientific tool, the development of the numerical ocean model PersianGulfOceanicModel (ZSF974) was initiated with the aim of predicting and calculating the physical parameters of the Persian Gulf.

This study presents the development process of the ocean numerical model "PersianGulfOceanicModel (ZSF974)" [11]. The design and development of the model are based on the technical principles of the Basic Oceanic Model (BOM) [13]. Therefore, the PersianGulfOceanicModel (ZSF974) can be considered an advanced and expanded version of the BOM model, designed to simulate real ocean environments.

The method used for designing the model allows its application to any hypothetical or real basin, whether closed or open. Another advantage of this model is the possibility of comparison with similar models developed by other researchers, as well as the superior algorithm employed in its design, which ensures accurate predictions by properly considering the relationships among the mathematical equations. Furthermore, the correct application of Nihoul's theory [14] regarding wind-induced surface stress effects on lower layers in multilayer environments has enhanced the accuracy of the model outputs.

This research was conducted in two phases: for laboratory oceanic basins (first phase) and for real oceanic basins (second phase). In the first phase [15], the technical aspects, along with the model results for laboratory oceanic basins, were presented and analyzed. In the present study, while reaffirming the technical details of PersianGulfOceanicModel (ZSF974), the model results for the real Persian Gulf are provided. In addition, different aspects of the results are discussed to identify potential improvements.

2. Method and Theoretical Framework

In designing this type of oceanic model, in addition to applying the governing physical principles of the atmosphere and ocean—such as Newton's laws, conservation of mass, conservation of salinity, and conservation of thermal energy—the first and second laws of thermodynamics and the equation of state for seawater are also utilized. To enable the model to account for non-flat bathymetry as in real ocean environments, the sigma vertical coordinate (σ) was used. In this study, the vertical coordinate is considered in the form introduced by Zamanian (2006) [13]:

$$\sigma = \frac{p - p_A}{p_b - p_A} \qquad (1)$$

where σ denotes the normalized vertical coordinate; p_b is the bottom pressure at any point in the ocean; p_A is the atmospheric pressure over the ocean surface; and p is the pressure at any point in the water column. In this

system, $\sigma = 0$ corresponds to the ocean surface, and $\sigma = 1$ corresponds to the ocean bottom. The values $0 < \sigma < 1$ represent intermediate levels.

The unit vectors in The Earth's Spherical Coordinates System with the sigma vertical coordinate can be defined as: $\mathbb{e}_\lambda$ is in the direction of increasing longitude λ, $\mathbb{e}_\phi$ is in the direction of increasing, the latitude ϕ, and $\mathbb{e}_\sigma$ is in the direction of increasing σ, downward. The unit vector $\mathbb{e}_\sigma$ is a variable unit vector. The metric components in this coordinate system are as follows:

$$\begin{cases} \delta s_\lambda = r\cos\phi\,\delta\lambda \\ \delta s_\phi = r\,\delta\phi \\ \delta s_\sigma = \dfrac{p_b - p_A}{\rho\, g}\,\delta\sigma \end{cases} \tag{2}$$

where $\delta_{s\lambda}$ is the arc length in the longitudinal direction, r is the radial distance from the Earth's center, ϕ is latitude, $\delta\lambda$ is the increment in longitude, $\delta_{s\phi}$ is the arc length in the latitudinal direction, $\delta\phi$ is the increment in latitude, $\delta_{s\sigma}$ is the length element in the vertical direction, p_b denotes the bottom pressure, p_A is the atmospheric pressure, ρ is the density, and g is the acceleration due to gravity. The velocity vector in this coordinate system is expressed as:

$$\mathbb{u} = u\,\mathbb{e}_\lambda + v\,\mathbb{e}_\phi + w\,\mathbb{e}_\sigma \tag{3}$$

The velocity components are:

$$\begin{cases} u = r\cos\phi\,\dfrac{D\lambda}{Dt} \\ v = r\,\dfrac{D\phi}{Dt} \\ w = \dfrac{p_b - p_A}{\rho\, g}\,\dfrac{D\sigma}{Dt} \end{cases} \tag{4}$$

Using equations (2), (3), and (4), the total material derivative of an arbitrary variable in this system is written as:

$$\frac{D\ldots}{Dt} = \frac{\partial\ldots}{\partial t} + \frac{u}{r\cos\phi}\frac{\partial\ldots}{\partial\lambda} + \frac{v}{r}\frac{\partial\ldots}{\partial\phi} + \dot{\sigma}\frac{\partial\ldots}{\partial\sigma} \tag{5}$$

In which $\frac{D\ldots}{Dt}$ is the total derivative, $\frac{\partial\ldots}{\partial t}$ is the local rate of change, $\frac{u}{r\cos\phi}\frac{\partial\ldots}{\partial\lambda}$ denotes the eastward advection, $\frac{v}{r}\frac{\partial\ldots}{\partial\phi}$ represents the northward advection, and $\dot{\sigma}\frac{\partial\ldots}{\partial\sigma}$ represents vertical advection or convection [13].

Based on the aforementioned concepts, the governing equations of the model can be reformulated in the Earth's spherical coordinate system with the sigma vertical coordinate. These governing equations include the eastward momentum equation, the northward momentum equation, the thermal conductivity equation, the temperature equation, the specific volume equation, the salinity equation, as well as the corresponding thermodynamic equations derived from the first and second laws of thermodynamics.

To complete the formulation of the model, additional closure equations are required. These include the hydrostatic equation, the geopotential equation, the bottom pressure tendency equation, the representative vertical velocity ($\dot{\sigma}$) equation, and the equation for calculating the radial distance of each point from the Earth's center. It is essential that all of these equations are expressed consistently in the spherical coordinate system with the sigma vertical coordinate.

When wind blows over the sea surface, momentum is transferred from the atmosphere to the ocean due to air–sea friction. As a result, wind speed decreases and surface ocean currents are generated.

The wind-induced surface stress depends approximately quadratic ally on wind speed, and represents the aerodynamic force per unit area exerted by the wind on the sea surface [16].

$$\boldsymbol{\tau}_s = c_d\,\rho_a\,(|\mathbb{v}_{\boldsymbol{a}}| - |\mathbb{v}_{\boldsymbol{s}}|)\,(\mathbb{v}_a - \mathbb{v}_s)\ \mathrm{Nm}^{-2} \tag{6}$$

where $\boldsymbol{\tau}_s$ is the surface stress, c_d is the (dimensionless) aerodynamic drag coefficient, ρ_a is the air density, $\mathbb{v}_{\boldsymbol{a}}$ is the wind velocity vector at 10 m above the sea surface, and $\mathbb{v}_{\boldsymbol{s}}$ is the surface current velocity vector.

According to Wu (1985), the aerodynamic drag coefficient is given by:

$$c_d = (0.8 + 0.065\,U_{10}) \times 10^{-3} \tag{7}$$

where U_{10} is the wind speed at a 10 meter elevation [17]. Bottom stress, is computed using the formulation proposed by Nihoul (1977) [14]:

$$\boldsymbol{\tau_b} = -m\,\boldsymbol{\tau_s} + C_D\rho_w\ |\mathbb{v}|\ \mathbb{v} \tag{8}$$

Where $\boldsymbol{\tau_b}$ is the bottom stress, $m = 0.7$ is the dimensionless scaling coefficient for surface stress, $\boldsymbol{\tau_s}$ is the surface stress, $C_D = 0.00211$ is the hydrodynamic drag coefficient, ρ_w is the water density, $|\mathbb{v}|$ is the magnitude of the depth-integrated current, and $\mathbb{v}$ is the depth-integrated velocity vector.

In general, the stress tensor in the spherical coordinate system with sigma vertical coordinate is expressed as:

$$\boldsymbol{\tau} = \begin{bmatrix} \tau_{\lambda\lambda} & \tau_{\lambda\phi} & \tau_{\lambda\sigma} \\ \tau_{\phi\lambda} & \tau_{\phi\phi} & \tau_{\phi\sigma} \\ \tau_{\sigma\lambda} & \tau_{\sigma\phi} & \tau_{\sigma\sigma} \end{bmatrix} \tag{9}$$

Each component represents the stress associated with velocity gradients along different coordinate directions [13]. For example, $\tau_{\lambda\sigma}$ corresponds to the stress associated with variations of vertical velocity, $\dot{\sigma}$, along the longitudinal direction; $\tau_{\sigma\phi}$ corresponds to the stress generated by variations of meridional velocity in the vertical direction; and $\tau_{\sigma\sigma}$ represents the stress associated with the changes in the vertical velocity indicator, $\dot{\sigma}$, in σ direction.

Figure 2 shows the structure of a multilayer ocean model in a spherical coordinate system with a sigma vertical coordinate. In this figure the schematic of the vertical orientation of an n-layer (level:$Nk = 2n + 1$) oceanic medium. The counter of the levels is k.

a) Odd values of k correspond to the layer boundaries, while even values represent the centers of the layers.

b) $k = 1$ represents the ocean surface (the first level), which corresponds to $\sigma = 0$.

c) $k = Nk$ represents the ocean floor (the last level), corresponding to $\sigma = 1$.

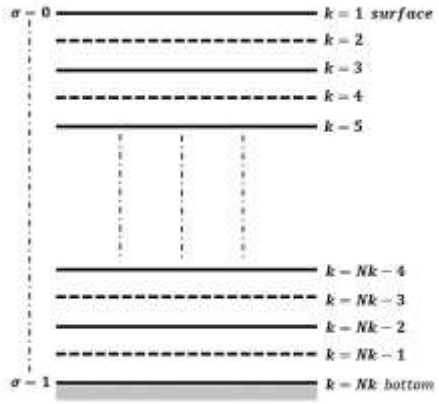

Figure 2- Vertical alignment scheme of a multilayer oceanic medium

In this study, the Modified Arakawa C-grid is employed for spatial discretization of the model domain [18]. To predict the future state of the ocean, the governing equations are solved numerically. These equations are first discretized using specific schemes, and a computer program was subsequently developed in C# to implement them.

The model is initialized with geometric conditions, including bed slope and elevation, along with other initial data.

Determining an appropriate time step is crucial for ensuring numerical stability in any modeling effort. The equations are solved and discretized using the finite difference method. Specifically, the two-step Lax-Wendroff scheme is applied to the advection terms, the Dufort-Frankel scheme to the diffusion terms, and the central difference method to the remaining derivatives. Additionally, the Matsuno scheme is employed to mitigate computational instabilities [19].

The Dufort-Frankel scheme is explicit and unconditionally stable. In contrast, the two-step Lax-Wendroff scheme is conditionally stable, requiring it to satisfy the Courant-Friedrichs-Lewy (C.F.L.) condition [20], While the C.F.L. condition is typically defined for a Cartesian coordinate system, it must be adapted for the Earth's spherical coordinate system with a sigma vertical coordinate, where it is expressed as:

$$\Delta t \leq min\left(\frac{r\,cos\,\phi\;\Delta\lambda}{u}, \frac{r\,\Delta\phi}{v}, \frac{\Delta\sigma}{\dot{\sigma}}\right) \qquad (10)$$

The simulation is initialized from a state of rest. Consequently, in the absence of forcing, the local time derivatives of the motion-inducing potentials are zero. Regarding the boundary conditions, the bottom and lateral boundaries are considered rigid, and a no-slip condition is applied [2]. Consequently, both the normal and tangential velocity components at these boundaries are set to zero, i.e.:

$$\mathbb{v}(\lambda, \phi, \sigma, t).\mathbf{n} = 0 \text{ and } \mathbb{v}(\lambda, \phi, \sigma, t).\mathbf{t} = 0 \qquad (11)$$

In the above equation, $\boldsymbol{t}$ and $\boldsymbol{n}$ are the unit tangential and normal vectors to the rigid boundary, respectively. The no-penetration condition at the bottom boundary requires that:

$$\sigma = 1 \quad \Rightarrow \quad u = v = \dot{\sigma} = 0 \qquad (12)$$

The dynamic boundary condition for the open boundary is considered as follows:

$$\frac{\partial p}{\partial \lambda} = \frac{\partial p}{\partial \phi} = \frac{\partial \Phi}{\partial \lambda} = \frac{\partial \Phi}{\partial \phi} = \frac{\partial p_b}{\partial \lambda} = \frac{\partial p_b}{\partial \phi} = 0 \qquad (13)$$

The kinematic boundary condition is expressed as:

$$u = \acute{u}, v = \acute{v}, \dot{\sigma} = \acute{\dot{\sigma}}, \rho = \acute{\rho}, \eta = \acute{\eta}, T = \acute{T}, s = \acute{s} \qquad (14)$$

Here, unprimed parameters represent the original environment, while primed parameters correspond to the conditions at the open boundary. Additionally:

$$\left(\frac{D\,\ldots}{Dt}\right)_{(\sigma=0)} = \left(\frac{D\,\ldots}{Dt}\right)_{(\sigma=1)} = 0 \qquad (15)$$

A key assumption in the development of the Basic Oceanic Model is the neglect of the term $-\vec{\Omega} \times \left(\vec{\Omega} \times \vec{r}\right)$ compared to other terms in the equations of motion formulated in the Earth's spherical coordinate system with a sigma vertical coordinate.

Applying specific conditions to the program and comparing its outputs with theoretical physical principles can also serve as an appropriate validation for the designed model. Calibration during the model execution for experimental basins identifies the model's weaknesses and leads to its improvement.

For model's implementation in laboratorial oceanic basins (even real medium), hypothetical (and approximate real) data are used as input to the program. The tidal force is considered as a sinusoidal function with a hypothetical amplitude. However, tidal force has been made to incorporate water level variations in the Strait of Hormuz (which is the open boundary of the real medium). The water level variations in the Strait of Hormuz have been extracted from the hydrography information database of the National Cartographic Center of Iran [21].

3. Results and Discussion

The preceding sections have described the design of the Persian Gulf Oceanic Model (ZSF974). The model's accuracy was validated in theoretical environments, with results showing consistency with the principles of ocean physics and agreement with previous research. This validation provides the basis for its implementation in a real-world environment, specifically the oceanic basin of the Persian Gulf (Figure 1) [15].

This section presents the results of the model's implementation in the Persian Gulf basin and discusses its validation. The model domain spans longitudes from 48.25°E to 56.5°E and latitudes from 24.25°N to 30.25°N, with bathymetry ranging from 9.02 m to 101 m. The depth of the basin in this area varies between a minimum of 9.02 meters and a maximum of 101 meters. The model uses a five-layer structure and the domain is discretized using the modified Arakawa C-grid scheme with a longitudinal and latitudinal resolution of 0.25 degrees. While the Courant-Friedrichs-Lewy (C.F.L.) condition permits a maximum time step of 95.95 seconds, a 60-second time step was used in practice to ensure stability.

In addition to hypothetical tides, the model was forced with real tidal data from the Hydrographic Information Database of the National Cartographic Center [21], covering the period from March 1 to June 30, 2018. Wind data were sourced from the European Centre for Medium-Range Weather Forecasts (ECMWF) database [22], and the wind forcing was applied concurrently with other factors, such as tides. To isolate the effects of specific factors, some experiments were initialized with uniform conditions: the basin temperature was set to 25 °C and salinity to 40 psu. All simulations of the Persian Gulf were initialized from a state of rest.

3.1. Results of the QuiescencetTest and the effects of neglecting Coriolis force and Earth's curvature.

The first simulation was a quiescence test, where no external forces were applied. The model was expected to maintain its initial state, with no changes in parameters or generation of currents over time. The model was run for ten years to confirm this quiescent state. A subsequent test examined the effect of neglecting the Coriolis force and Earth's curvature. In this scenario, when a constant force (e.g., uniform wind stress) was applied, the model produced a uniform current aligned with the applied force.

Following the successful validation from these two initial tests, the model was used to examine other influencing factors. Specifically, the effects of density gradients, wind, tides, and river runoff—both individually and in various combinations—were investigated. The results of some of these experiments are presented below.

3.2. Simulating the Effects of River Inflow on the Persian Gulf

This experiment investigates the effect of inflow from the Arvandrud and Mond rivers (Figure 1) on water circulation in the Persian Gulf. To isolate this effect, the simulation was run under stable conditions, excluding tidal, wind, and density gradient forces. The basin was initialized with a uniform salinity of 40 psu and a temperature of 25 °C. The Arvandrud River was prescribed an inflow with a temperature of 18 °C, salinity of 38.5 psu, and velocity of 1.14 m/s, while the Mond River had an inflow with a temperature of 20.0 °C, salinity of 22.1 psu, and velocity of 0.5695 m/s. The results of the simulation at the end of the fifth day are presented below:

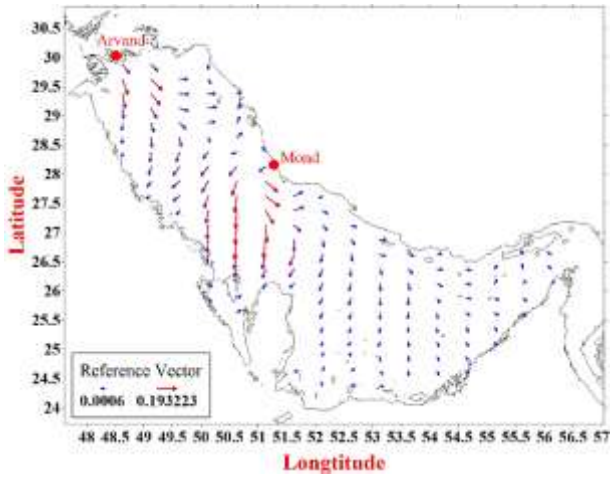

Figure 3- Current field at the center of the first layer after five days of simulation, forced only by runoff from the Arvandrud and Mond rivers.

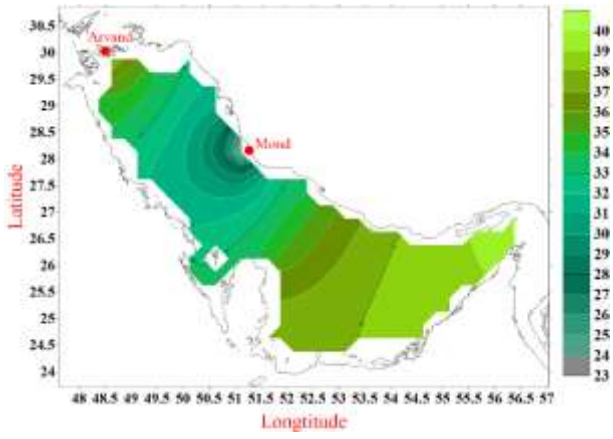

Figure 4- Salinity field at the center of the first layer after five days of simulation, forced only by runoff from the Arvandrud and Mond rivers.

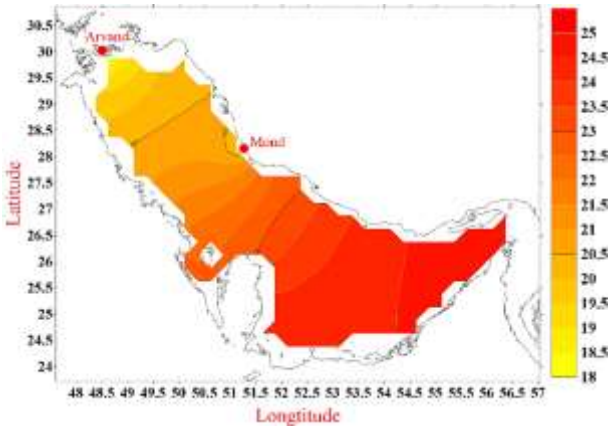

Figure 5- Temperature field at the center of the first layer after five days of simulation, forced only by runoff from the Arvandrud and Mond rivers.

Figure 4 and 5 illustrate the dominant effects of the Mond and Arvandrud rivers on the salinity and temperature of the Persian Gulf, respectively. These effects stem from the distinct temperature and salinity characteristics of the river inflows compared to the ambient Gulf water. The current field (Figure 3), however, shows that the river inflows collectively generate a counterclockwise circulation within the basin. The outflow from the Arvandrud River is observed to deflect to the right after entering the Gulf, impacting the coasts of the United Arab Emirates. A similar pattern is observed for the Mond River inflow. This suggests that, in the absence of other forces such as tides, wind, or density gradients, the Mond River inflow also affects the coasts of the United Arab Emirates and Bahrain.

3.3. Simulating the Effects of Wind and Density Gradients on the Persian Gulf

In this experiment, the model is initialized with a surface temperature of 30°C and a surface salinity of 36 psu. Temperature decreases by 0.25°C and salinity increases by 0.5 psu with each successive layer. A uniform westerly wind with a speed of 10 m/s was applied to the surface for 40 days. The resulting velocity, salinity, and temperature fields, as well as the deviation from hydrostatic balance at the end of the fifth day, are presented below:

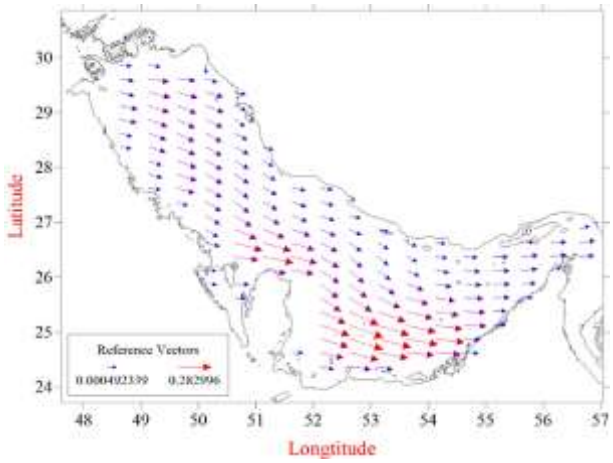

Figure 6- Current field at the mid-depth of the first layer after five days of simulation, forced by a 10 m/s westerly wind.

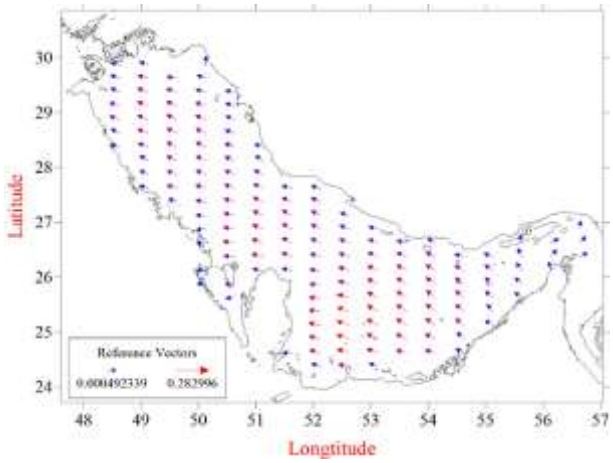

Figure 7- Current field, mid-level of the fifth layer, the end of the fifth day of model execution forced by 10 m/s westerly wind.

As expected, the surface current vectors are deflected to the right of the wind direction due to the Coriolis effect. In the bottom layer, the current vectors are oriented approximately opposite to those in the surface layer. Figure 8 shows a lower sea level in the western Persian Gulf compared to the eastern part, a pattern consistent with the observed current field. Consequently, higher salinity and lower temperatures are expected in the western basin (Figure 9 and 10).

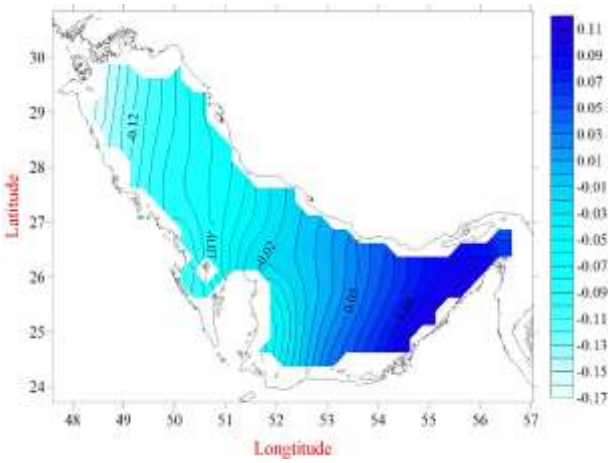

Figure 8- Isopleths of departure from static equilibrium at the mid-depth of the first layer after five days of simulation, forced by a 10 m/s westerly wind.

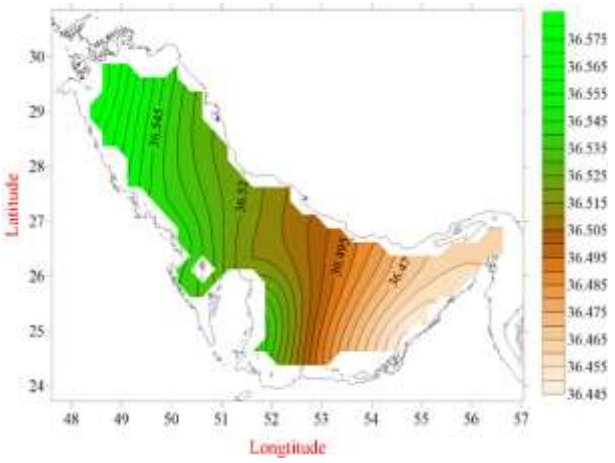

Figure 9- Salinity field, mid-depth of the first layer, the end of the fifth day of model execution forced by 10 m/s westerly wind.

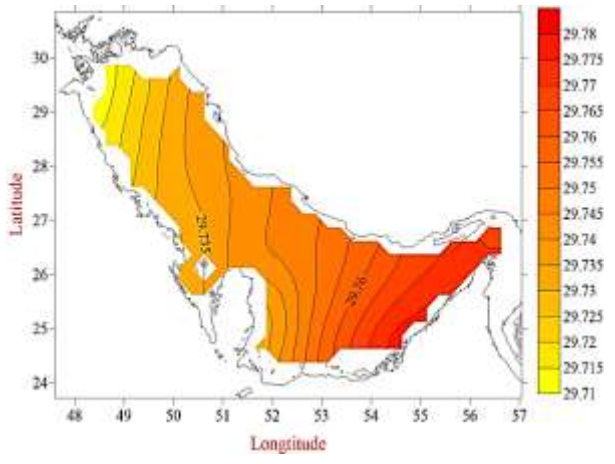

Figure 10- Temperature field at the mid-depth of the first layer after five days of simulation, forced by a 10 m/s westerly wind.

Due to the open boundary, the persistent wind forcing is expected to maintain a lower sea level, especially in the upwind region. The results after 30 days of the simulation are presented below:

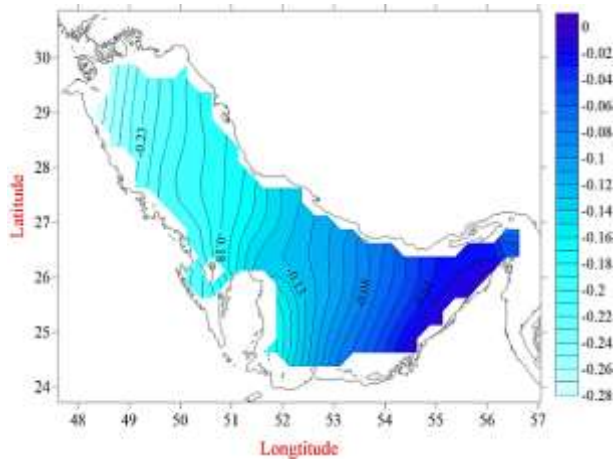

Figure 11- Isopleths of departure from static equilibrium at the mid-depth of the first layer after 30 days of simulation, forced by a 10 m/s westerly wind.

The current field stabilizes in terms of direction within the first five days, and the surface outflow from the Strait of Hormuz as well as the inflow at the bottom into the Persian Gulf continues. A comparison of the results from days 30 and 40 (Figure 11 and 12) confirms this observation

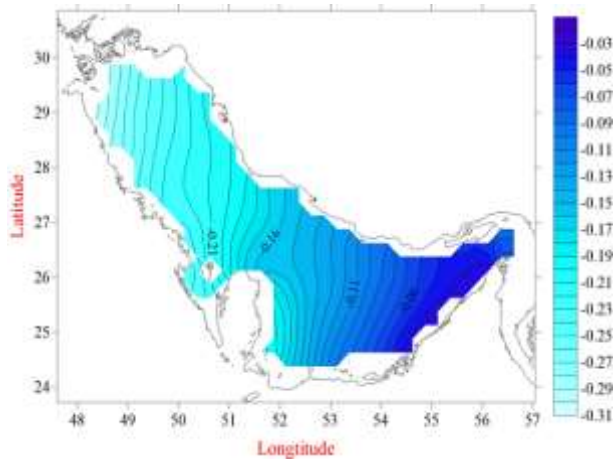

Figure 12- Isopleths of departure from static equilibrium, mid-level of the first layer, the end of day 40 of model execution forced by 10 m/s westerly wind.

Salinity and temperature also continue to diffusion, as shown in Figure 9 and Figure 10, contributing to changes in sea level and current patterns. However, the rate of these changes decreases over time. The result of this experiment indicates the dominance of wind forcing over the density gradient in this oceanic medium.

3.4. Analysis of the results of the simulation of the tidal effect and density gradient in the Persian Gulf

Tide, as a periodic factor, imposes a periodic dynamic on the oceanic medium. In this experiment, the tidal force affects the medium in the absence of wind and river inflow. The sea surface temperature is set at 30°C, decreasing by 0.25°C per below level, and the surface salinity is assumed to be 36 psu, increasing by 0.5 psu per below level. Under these conditions, the model has

been run for 60 days. Below are some results from day 58 of the model run:

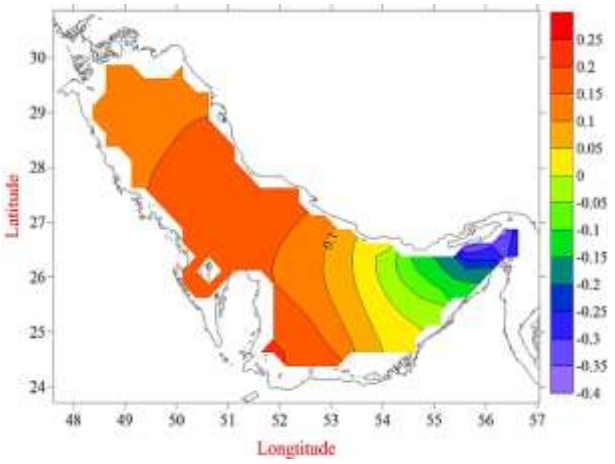

Figure 13- Isopleths of departure from static equilibrium, mid-level of the first layer, day 58 of the model run – hour 6, forced by tide.

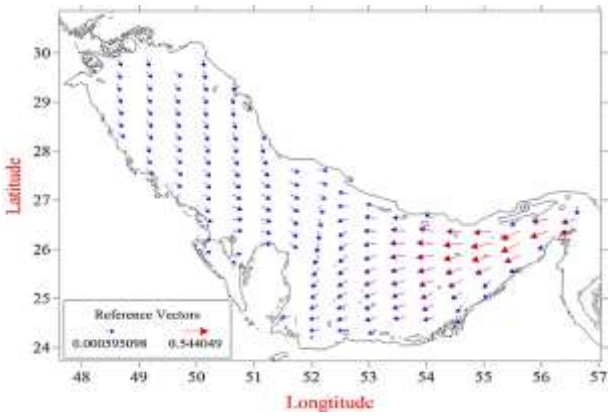

Figure 14- Current field, mid-level of the first layer– day 58 of the model run, hour 12, forced by tide.

The maximum observed current during this period was 0.998 m/s, and the maximum total change in water elevation relative to the static equilibrium was 3.4 m. Results indicate the dominance of tidal force compared to the force resulting from density difference. The current fields and isopleths of departure from static equilibrium (Figure 13 and Figure 14) show that the tide is dominant in the meridian region. This finding can also be obtained by examining the temporal changes in the departure from static equilibrium at a specific point (Figure 15).

Additionally, the current fields indicate that the tidal wave, after entering the Strait of Hormuz, enters the Persian Gulf parallel to the northern boundary, as the current vectors are aligned well parallel to the boundaries.

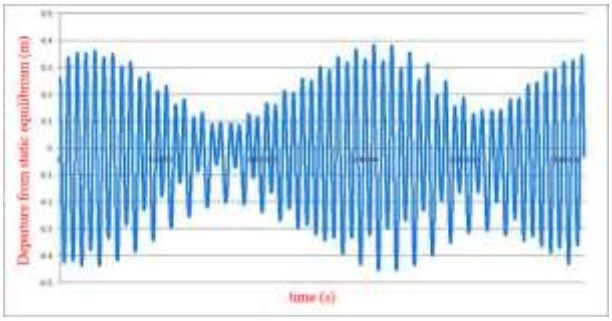

Figure 15- Water level fluctuations over time at 26°22'30"N, 54°52'30"E in April 2018.

By comparing the isopleths of departure from static equilibrium with the current fields, it can be understood that if an observer looks at the tidal current in the direction of flow, the maximum amplitude will be to their right, tending to create a counter-clockwise motion in the environment. Overall, the presence of the Kelvin wave due to tidal entry, as well as the dominance of tidal force over the force resulting from density difference, are observed in the results.

Results indicate that the effect of tidal force in the western half of the Persian Gulf is weaker than in the eastern half.

3.5. Investigating the Results of Simulating the Effects of Wind, Tide, and Density Difference in the Persian Gulf

In this experiment, the salinity of the Persian Gulf at the surface is set at 36 psu, with a 0.5 psu increase in salinity per below level, and the temperature at the surface is assumed to be 30°C, with a 0.25°C decrease per below level. The wind data extracted from the ECMWF website is from March 1, 2018, to March 31, 2018 (March 2018), and the tidal data for the same dates was obtained from the Hydrography website of the National Cartographic Center. The model was run for 30 days under the stated conditions. Below are some results from this run:

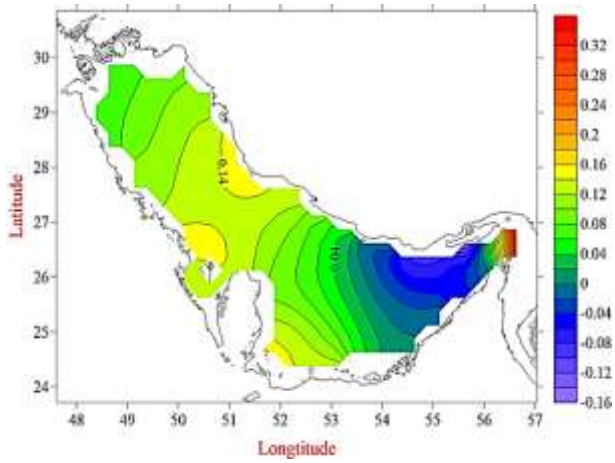

Figure 16- Isopleths of departure from static equilibrium at the mid-depth of the first layer at hour 6 of day 30, forced by tides, wind, and density gradients.

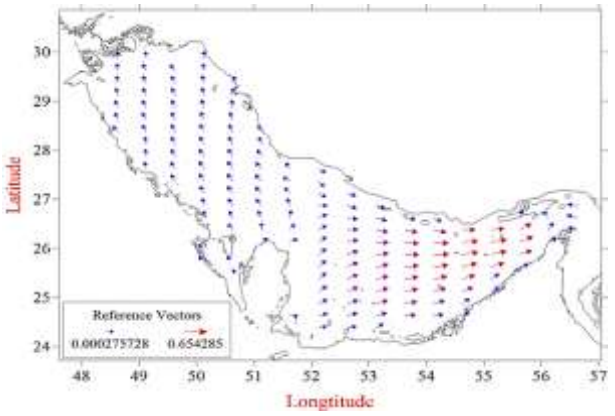

Figure 17- Current field at the mid-depth of the first layer at hour 6 of day 30, forced by tides, wind, and density gradients.

Analysis of the departure from static equilibrium fields shows that as the tide propagates into the basin, a counterclockwise circulation develops along the boundaries, with the maximum and minimum sea levels consistently occurring near the coast (Figure 16). Moreover, the current vectors at these locations are well-aligned with the boundaries (Figure 17), indicating that the normal component of the current is negligible. This leads to the conclusion that tidal forcing dominates the circulation in this experiment. This finding is also supported by the analysis of temporal variations in sea level at a specific point (Figure 18). Furthermore, the analysis reveals the presence of an amphidromic point within the basin (Figure 16).

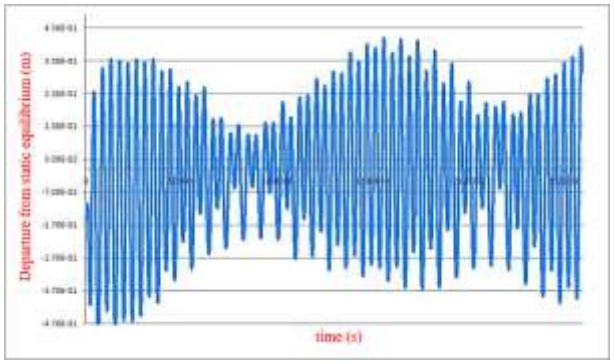

Figure 18- Time series of sea level variations at 26°22′30″ N, 54°52′30″ E in March 2018.

It is also evident that both tidal currents and tidal elevations are greater in the eastern part of the Persian Gulf compared to the western part. The maximum simulated current in this experiment is 0.924 m/s, occurring in the Strait of Hormuz, while the maximum change in sea surface elevation relative to static equilibrium is 3.3 meters. The analysis of salinity and temperature fields also yielded useful results, with examples presented below.

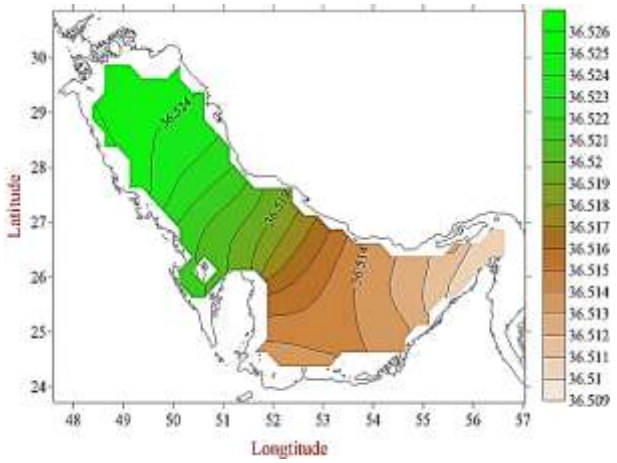

Figure 19- Salinity field at the mid-depth of the first layer at hour 6 of day 30, forced by tides, wind, and density gradients.

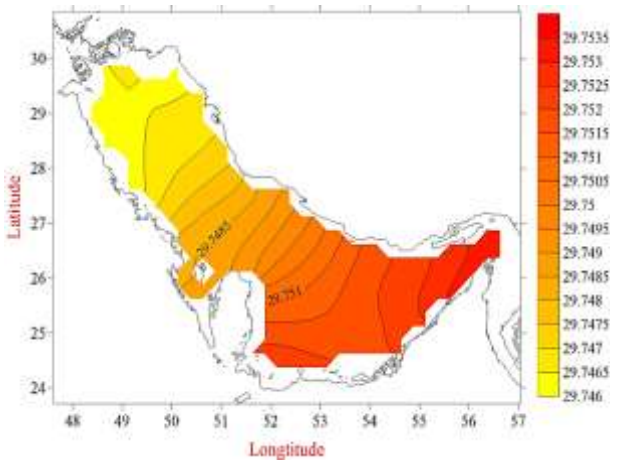

Figure 20- Temperature field at the mid-depth of the first layer at hour 6 of day 30, forced by tides, wind, and density gradients.

5. Conclusions

This study presents the development and validation of the Persian Gulf Oceanic Model (ZSF974), a three-dimensional numerical model designed to simulate the physical dynamics of the Persian Gulf. After successful validation against theoretical principles, the model was applied to the real-world environment of the Persian Gulf to investigate the effects of various forcing mechanisms.

The model's performance was confirmed through several key experiments. **Simulations of river inflow** from the Arvandrud and Mond rivers demonstrated their distinct impacts on salinity and temperature, and successfully reproduced the deflection of the Arvandrud plume towards the coasts of the United Arab Emirates, consistent with previous research [23]. In experiments examining **wind and density gradients**, the model accurately simulated Ekman dynamics [24], including the right-hand deflection of surface currents and the reversal of flow at depth, alongside realistic upwelling patterns. The results confirmed that, under the tested conditions, wind forcing dominated over density-driven forces

Analysis of tidal effects revealed the propagation of a Kelvin wave along the northern boundary, the

formation of an amphidromic point, and the overall dominance of tidal forcing over both wind and density gradients. This was further corroborated in a final, comprehensive simulation incorporating all three factors, where the semidiurnal nature of the tide and its dominant effect on circulation were clearly evident

The PersianGulfOceanicModel (ZSF974) has proven capable of accurately simulating the complex physical behavior of the Persian Gulf. A key advantage of this model is its ability to provide detailed physical parameter fields in lower water layers. However, long-term simulations indicate that enhancing the open boundary conditions and incorporating more precise bathymetric data are critical for improving the model's predictive accuracy. The groundwork has been laid for future enhancements, including the application of this model to other similar semi-enclosed basins with complex bathymetries.

Acknowledgment (Optional): The authors would like to express their sincere appreciation to the esteemed, Dr. Mohammad Taghi Zamanian, for his invaluable support. As the academic advisor, he provided comprehensive guidance in numerical modelling and played a fundamental role in the development of the present model. So, they would like to thank the National Institute of Oceanography for providing the facilities and library resources necessary for this research. We are especially grateful for the support and cooperation of the director and the vice president for research.

8. References

1- Khaleghi Zavare, H., (1992). *Development and application of a non-linear barotropic model for the wind and tide, driven circulation in the Persian Gulf* (Doctoral dissertation, University of the Philippines)

2- Zamanian, M., T., (1994). *Three Dimensional Models for Persian Gulf*, (Doctoral dissertation, University of the Philippines)

3- Sadrinasab, M. and Kenarkoohi, K., (2009). *Numerical modelling of sound velocity profile in different layers in the Persian Gulf*, Asian journal of applied sciences, 232-239.

4- Sadrinasab, M., (2009). *Three-Dimensional Numerical Modeling Study of the Coastal Upwelling in the Persian Gulf*. Research Journal of Environmental Sciences, 3: 560-566. DOI: 10.3923/rjes.2009.560.566,

5- Pous, S., Carton, X., and Lazure, P., (2012). *A process study of the tidal circulation in the Persian Gulf*, Open Journal of Marine Science, 2(4), 131-140, DOI: 10.4236/ojms.2012.24016.

6- Azizpour, J., Chegini, V., Khosravi, M. and Einali, A., (2014). *Study of the physical oceanographic properties of the persian gulf, strait of hormuz and gulf of oman based on PG-GOOS CTD measurements*, Persian Gulf Scientific Research Journal, *5*(18), 37-48.

7- Delbari, A., and Sheikhbahaei, A., (2022). *Numerical modeling of underwater acoustic wave using Differential Quadrature Method*, International Journal Of Coastal, Offshore And Environmental Engineering (ijcoe), 7(2), 49-54., doi: 10.22034/ijcoe.2022.155146.

8- Mahpeykar, O. and Khalilabadi, M. R., (2021). *Numerical modelling the effect of wind on Water Level and Evaporation Rate in the Persian Gulf*. International Journal of Coastal, Offshore & Environmental Engineering (IJCOE), 6(1), 47-53, Doi: 10.22034/ijcoe.2021.149358

9- Hosseini, S. M. and Soltanpour, M., (2021). *Tide characteristics and tidal wave propagation in the Persian Gulf*, Ocean Science Discussions, 1-36.

10- Pirooznia, M., Raoofian Naeeni, M., Atabati, A., and Tourian, M. J. (2022) *Improving the Modeling of Sea Surface Currents in the Persian Gulf and the Oman Sea Using Data Assimilation of Satellite Altimetry and Hydrographic Observations*. Remote Sensing, 14(19), 4901. https://doi.org/10.3390/rs14194901

11- Fallahi M., Zamanian M.T. and Sadrinasab M. (2019). *Design of Five Layers Oceanic Numerical Model for Persian Gulf*. PHD Thesis. Department of physical oceanography, Faculty of Marine Science and Oceanography, Khorramshahr University of Marine Science and Technology, Iran. 183p. [In Persian]

12- Zamanian M.T, Sadrinasab M. & Fallahi, M., (2022). *Designing a Numerical Model to Study the Effect of Tide and Wind in a Theoretical Basin in Similarity to Persian Gulf*, Journal of Marine Science and Technology, 27-38, 21(1), doi:10.22113/jmst.2019.149922.2203, [In Persian]

13- Zamanian, M. T. (2006). *Project of base oceanic model two layered*, Research Institute of Methodology and Atmosphere Science, Tehran, Iran. [In Persian]

14- Nihoul, J., C., J., (1977). *Three-dimensional model of tides and storm surges in a shallow well-mixed continental sea*, Dynamics Atmosphere Ocean, 2, 29-47.

15- Fallahi, M. , Zamanian,M. T. and Sadrinasab, M. (2025). *Development of Oceanic Numerical Model for Persian Gulf (part 1)*. International Journal of Coastal, Offshore And Environmental Engineering (ijcoe), 10(3), 18-29. doi: 10.22034/ijcoe.2025.522670.1175

16- Thorpe, S., A., (2009). *Elements of Physical Oceanography*, Boston, Elsevier, 647 pp

17- Wu, Y., (1985). Wu, J., 1982: *Wind stress coefficients over sea surface from breeze to hurricane*. J. Geophysics. Res., 78, 9704-9706.

18- Estoque, M., A., (1963). *A numerical model of the atmospheric boundary layer*, Journal of Geophysical Research, 68(4), 1103-1113, https://doi.org/10.1029/JZ068i004p01103

19- Haltiner, G.J. & Williams, R.T., (1980). *Numerical prediction and dynamic meteorology (2nd edition)*, John Wiley & sons, pp. 496, ISBN-10: 0471059714

20- Kämpf, J., (2009). *Advanced Ocean Modelling, Flinders University, School of the Medium*, PO Box 2100 Adelaide SA 5001, Australia, 193p.
21- Hydrographic Management of National Cartographic Center of the Islamic Republic of Iran, 1983, Access in: http://iranhydrography.ncc.org.ir/homepage.aspx?site=iranhydrography.ncc.org&tabid=6144&lang=fa-IR, Access Date: August 2018.
22- European Centre for Medium-Range Weather Forecasts (ECMWF). 1975. Available at: https://www.ecmwf.int/en/forecasts/datasets. Accessed September 17, 2018.
23- Emery, K., O., (1956). *Sediments and water of the Persian Gulf*, AAPG. Bull. 40 2354–2383
24- Apel, J. R., (1999). *Principles of Ocean Physics,* San Diego, Academic Press, 634 pp